Cohesional behaviours in volcanic material and the implications for deposit architecture.

[1] Nemi Walding, [1] Rebecca Williams, [2] Pete Rowley, [3] Natasha Dowey

[1] School of Environmental Sciences, Energy and Environment Institute.

University of Hull,

Cottingham Road, Hull. HU6 7RX

[2] University of Bristol

[3] Sheffield Hallam University

Email: n.walding-2021@hull.ac.uk

ORCID:

N. Walding (0000-0002-4584-1319)

R. Williams (0000-0002-8203-9982)

P. Rowley – (0000-0002-8322-5808)

N. Dowey – (0000-0002-9231-4781)

Acknowledgements: N.W was supported by the EU Horizon 2020 Programme (Project GEOSTICK 712525). We thank Gilbertson et al., (2020) at the University of Bristol for the use of the fluidisation chamber. Ulrich Küppers is thanked for suppling the volcanic material used in these experiments.

Abstract

Pyroclastic Density Currents (PDCs) are hazardous, multiphase currents of heterogeneous volcanic material and gas. Their high mobility can be partially attributed to fluidisation mechanisms. Moisture (as liquid or gas) can enter a PDC through external (e.g., interaction with bodies of water) or internal (e.g., initial eruptive activity style) processes and presence of moisture can be recorded within distinct deposit layers. We use analogue experiments to explore the behaviour of volcanic material with increasing moisture percentages from 0.00 – 10.00%. Our results show that: 1) the cohesivity of ignimbrite material changes with the addition of small amounts of moisture; 2) Small increases in moisture content change the flow behaviour from a free-flowing material to a non-flowable material; 3) changes in moisture can affect the formation of gas escape structures, and fluidisation profiles, 4) gas flow through a deposit can lead to a moisture profile and resulting mechanical heterogeneity within the deposit and 5) where gas escape structure growth is hindered by cohesivity driven by moisture, pressure can increase and release in an explosive fashion. This work highlights how a suite of dynamic and varied gas escape morphologies can form within the deposit resulting from moisture content heterogeneity, explaining variation in gas escape structures as well as providing a potential mechanism for secondary eruptions.

Key Words: Cohesion, Gas escape, Fluidisation, Secondary eruptions, Pyroclastic Density Currents, Deposit

Introduction

Pyroclastic density currents (PDC) are hazardous, multiphase, rapidly moving, often high-temperature currents of heterogeneous volcanic material and gas. The high mobility of PDCs has been attributed to fluidisation (Sparks, 1976; 1978; Wilson, 1984; Branney and Kokelaar, 1992, 2002; Breard et al., 2023) where the upward movement of gas supersedes the force of gravity and supports the flow (Sparks, 1976; Branney and Kokelaar, 2002; Cocco et al., 2014). The ability of a current to fluidise and flow can be described by its 'flowability', which depends upon interparticle forces (Van der Waals, electrostatic or capillary forces). These forces can be influenced by bulk composition and material physical properties such as particle size, density, shape, and moisture content (Rios., 2006; Leturia et al., 2014).

Fluidisation in PDCs can be initiated during formation and maintained throughout the course of the flow by continued fluidisation mechanisms such as substrate evaporation (i.e., steam generated from interaction with surfaces with moisture content or bodies of water), bulk self-fluidisation or ambient air entrainment (Sparks, 1978; Branney and Kokelaar, 2002; Chedeville and Roche, 2015; Breard et al., 2023). Sedimentation fluidisation (or, hindered settling) and particle-self fluidisation is where compaction from particle settling and sorting causes interstitial fluid movement. On or after deposition, the material will defluidise which can lead to segregation of material through gas escape structures, which form concentrated areas of particle sorting (i.e., fines depleted elutriation pipes) and segregation of particles (Wilson, 1980; Cas and Wright, 1991).

Previous analogue investigations into fluidisation behaviours of volcanic material and segregations structures have been completed on dry (0%; Wilson 1980; 1984) and saturated (80+-15%; Roche et al., 2001) natural ignimbrite (herein defined as the deposits of PDCs, typically consisting of poorly-sorted ash and pumice or scoria (Giordano & Cas 2021). Experiments completed by Wilson (1980; 1984) used non-cohesive, poorly-sorted ignimbrite mixtures, and added an influx of gas into the deposit. This resulted in poor fluidisation behaviours and the formation of gas escape structures determined by particle size and density. Roche et al (2001) explored contrasting aqueous fluidisation in a water-saturated deposit of volcanic material. These results determined that fluid-escape pipes form readily with low water flux and contain localised segregation of particle sizes and densities. From both experiments, we can determine that natural ignimbrite material will demonstrate aggregative (i.e., inhomogeneous; Branney and Kokelaar, 2002) fluidisation resulting from particle size and density range, irrespective of the fluidising medium.

Understanding how moisture impacts powder material has important industrial applications. Experiments have explored fluidisation behaviours of industrial material with the addition of small volumes of moisture (i.e., through adsorption of ambient humidity). With the introduction of moisture into a material, Van der Waals forces are no longer dominant, and liquid bridges connect particles through capillary cohesion; resulting in poor fluidisation behaviours (Wormsbecker and Pugsley, 2008; Ludwig et al., 2020; Yehuda and Kalman, 2020). A study by Wormsbecker and Pugsley (2008) looked at gas fluidisation behaviours on a semi-saturated (30, 20, 15 and 5 wt.% moisture) powder. Results showed a dominant change in fluidisation behaviour

associated with the addition of moisture, which were observed in conjunction with the drying states of the material from 30 to 5 wt.%.

The experiments detailed herein experimentally assess the impact of the addition of small volumes of moisture within natural volcanic material. We identify the resulting variations in terms of fluidisation and particle segregation behaviours.

Moisture in PDCs and their resulting deposits

Moisture (i.e., water vapour or liquid water) can enter a PDC system during formation at source or as they propagate (**Error! Reference source not found.**). Eruption columns can be water-rich due to phreatomagmatism (Self and Sparks, 1978; Hurwitz, 2003; Houghton et al., 2015) or atmospheric conditions (Vecino et al., 2022). During transport, internal clasts of juvenile magma will exsolve and release water vapour and other volatiles. Experiments have highlighted how magmatic clasts may still hold residual water content of 0.6 – 0.8 wt. % during transport (Sparks et al., 1978).

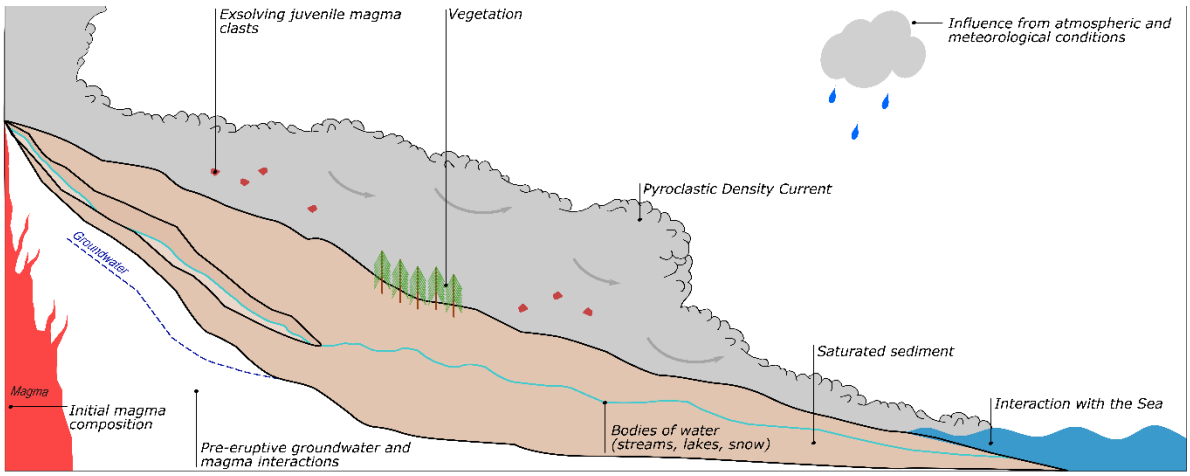

Fig.1 a PDC interacting with sources of moisture across a landscape which have the potential to enter the PDC system and resulting deposits.

Externally, moisture may be introduced through a dynamic mix of atmospheric (e.g., humidity; Pepin et al., 2017; Camuffo, 2019), topographic (e.g., height; Barclay et al., 2006; Duane et al., 2008; Hartman, 2016), climatic (e.g., global location; Barclay et al., 2006) and meteorological conditions (e.g., precipitation). Furthermore, periods of intense rainfall have been suspected and observed to affect the onset of volcanic activity (Barclay et al., 2006; Sahoo et al., 2022 and references therein). Matthews et al., (2009) documented that within 24 hours of heavy rainfall, the probability of lava dome collapse at Soufriere Hills Volcano, Montserrat (during the period 1998-2003) increased, resulting in higher moisture availability to the resulting PDCs.

Interaction with external bodies of water (i.e., streams, lakes, sea, snow; Dartevelle et al., 2002; Cole et al., 1998; 2002), water saturated substrate (Moyer and Swanson, 1987; Brown and Branney, 2013; Gilbertson et

al., 2020) or by the incorporation of vegetation (as observed in Mount Pelé, 1902; Mount St Helens, 1980; Montserrat, 2002 and Fuego Volcano, 2018) can also contribute to moisture within the flow system. Therefore, we expect moisture content in PDCs to be highly variable in time and space.

The presence of moisture within PDCs can be demonstrated through varying degrees within an ignimbrite deposit. Moisture has been linked to the formation of wet ash aggregates (e.g., pellets) in ignimbrite deposits (Brown et al., 2010), by the presence of elutriation pipes that are derived from areas of evaporating moisture (i.e., vegetation or water-laden sediments) or by secondary hydroeruptions forming in deposits overlying moisture-rich areas (e.g., Mount St. Helens; Moyer and Swanson, 1987). The influence of these relatively small additions of moisture into a PDC system has been largely ignored in analogue and experimental studies, due to the difficulty associated using and controlling the characteristics of cohesive material. Therefore, prior to the experiments, material is often dried to remove any residual moisture (Druitt et al., 2004, 2007; Girolami et al., 2008; 2015).

Capillary Cohesion

The presence of moisture in a PDC, or in a subsequent deposit, will result in cohesional forces within the interparticulate space. A PDC can reach temperatures > 1000°C and the resulting deposit can maintain high temperatures for extended periods of time (Dufek, 2016; Riehle et al., 1995), and it has been assumed that at these temperatures the dominant cohesive forces will be electrostatic and Van der Waals forces (Branney and Kokelaar, 2002). However, with increasing distance and entrainment, temperatures will lower (Benage et al., 2016) and the introduction of moisture will likely lead to the formation of capillary bridges ('capillary condensation'; Ma et al., 2019), resulting in a change of the dominant interparticulate forces . This is observed by Telling et al., (2013), where electrostatic attraction has been observed to be dominant only where humidity was lower than 71% and by Chigira and Yokoyama (2005), where capillary cohesion became the dominant cohesive force with the addition of moisture into a granular material.

Previous studies have shown that an increase in water content and moisture leads to a drastic change in the physical properties of a bulk material. For example, in sands, capillary forces were seen to affect the tensile strength of a material until reaching a water saturated state (Kim and Sture, 2008; Chen et al., 2021). Therefore, at lower temperatures, it is highly likely that the introduction of moisture into the dynamic (pyroclastic current) and static (deposited sedimentary packages from a current) regions will introduce variations in material properties (e.g., as a sedimentary package). Changes in tensile strength may determine how resistant a material is to shear and erode and are important in understanding the flow properties of a material (Pierrat and Caram, 1997; LaMarche et al., 2016). Within a PDC deposit, such changes may also influence defluidisation through gas escape.

Here, we investigate how capillary cohesion, through the introduction of water, may affect volcanic material in a static state. We present the results of analogue experiments that test how changes in cohesion of volcanic

material affects its fluidisation. Our results provide new and novel insights into the variation of gas escape behaviours in a defluidising PDC deposit.

Methodology

Source material and Sample Preparation

A range of unconsolidated material collected in 2009 from the 2006 Tungurahua, Ecuador, eruptions (provided by U. Küppers, LMU Munich) has been subjected to a range of characterisation tests to elucidate flowability properties and variations with moisture content.

The ignimbrite material is dark grey/brown and andesitic in chemistry (Eychenne et al., 2012) and samples were sieved into varying size fractions, with specific particle size distributions created for the suite of analysis. All samples were dried in an 80°C oven for 24 hours to ensure the removal of residual and adsorbed moisture and agglomerations were broken-up by sieving prior to addition of water. For the series of characterisation tests, water was added to the samples based on weight percentage (0.00, 0.25, 0.50, 1.00, 2.50, 5.00, 7.50, 10.00 %). Samples were stirred thoroughly to ensure a homogeneous moisture distribution.

Material characterisation and cohesive behaviour tests

Particle Size Analysis

Particle analysis of the ignimbrite material was undertaken using a CAMSIZER X2. This uses particle imaging to build particle shape and size characteristics for dry samples. Particles were sieved prior to using the CAMSIZER with samples <1000 µm were used. Any results from the CAMSIZER erroneously returned as >1460 µm were removed.

Geldart's Classification of Powders

Geldart (1973) classified powders into four distinctive groups (A-D) defined by fluidisation behaviours, which vary dependent on particle size and density; resultant flowability properties are described as 'very poor' to 'excellent'. Group C, the finest material (< 20 µm), is dominated by interparticulate forces. Group D (>1 mm) requires an increased gas velocity to fluidise. Group C and D present passable to very poor fluidisation behaviours and would typically express as slugging, channelling, and spouting behaviours (Leturia et al., 2014). Group A (30 – 100 µm) and B (100 µm – 1mm) powders show the best fluidisation behaviours overall and are most likely to have good flowability, typically expanding under fluidisation.

Volcanic materials used in these experiments (Fig. 2) have particle size distributions from 2.5 to 1000 µm. and should readily exhibit fluidisation behaviours typically of Groups A and B in Geldart's classification.

Bulk and Tapped Density

Bulk and tapped density measurements describe the mass and volume ratio of a material, without and with packing respectively (Amidon et al., 2017). Tapped density experiments remove interparticulate voids. The differences within the bulk and tapped density measurements correspond to the cohesive properties of the particles (Deb et al., 2018) and can be affected by shape and size of material (Amidon et al., 2017).

Bulk and tapped density were calculated for dry sample herein to characterize cohesive behaviour prior to the addition of water (method adapted from USP: Bulk and Tapped Density of Powders, 2015).

Bulk density was obtained by pouring 100g of the volcanic material into a 250mL cylinder and levelling where needed. The unsettled volume was measured, and bulk density calculated using Equation 1. This procedure was completed three times per sample.

$$\rho_{b=\frac{m}{V_0}} \quad [1]$$

m = *mass (g)*

V_o = *unsettled apparent volume (mL)*

The cylinder was tapped at 150 taps/min, with volume measured every minute until leveled. Using the unsettled apparent volume and final tapped volume, the tapped density (Eq. 2), Carr's Index (Eq. 3) and the Hausner ratio (Eq. 4) could be calculated.

$$\rho_{t=\frac{m}{V_f}} \quad [2]$$

m = *mass (g)*

V_f = *final tapped volume (mL)* (Moondra *et al.*, 2018)

The Carr's Index and Hausner Ratio are indicative of flowability and interparticulate behaviours (Hausner, 1981) and are a useful tool in determining a materials ability to fluidise and flow (Table 1) .

The Carr's Index measures the strength and compressibility of a material (Equation 3; Moondra *et al.*, 2018).

$$CI = 100\left(\frac{\rho_t - \rho_b}{\rho_t}\right) \quad [3]$$

The Hausner Ratio determines how certain powders will behave i.e., flowability and fluidisation (Equation 4, Yu and Hall, 1994; Abdullah and Geldart, 1999).

$$HR = \frac{\rho_t}{\rho_b} \quad [4]$$

Table 1 Relationship between Carr's Compressibility Index, Hausner Ratio, and flowability behaviours. From (Gorle and Chopade, 2020).

CI	HR	Flowability
≤10	1.00 – 1.11	Excellent
11 – 15	1.12 – 1.18	Good
16 – 20	1.19 – 1.25	Fair
21 – 25	1.26 – 1.34	Passable
26 – 31	1.35 – 1.45	Poor
32 – 37	1.46 – 1.59	Very Poor
> 38	>1.60	Very Very Poor

Angle of Repose

The Angle of Repose (AoR) refers to the static friction coefficient and the angle of internal friction, and can be investigated through static (funnel) and dynamic (rotating cylinder drum) methods (Al-Hashemi and Al-Amoudi, 2018). AoR results are attributed to understanding the flowability of a material (Table 2).

Table 2 Flowability based on angle of repose results (Al-Hashemi and Al-Amoudi., 2018).

Flowability	Angle of Repose (°)
Very free flowing	<30
Free flowing	30 - 38
Fair to passable flow	38 - 45
Cohesive	45 - 55
Very Cohesive (non-flowing)	>55

To determine the static angle of repose (SAoR) for each experiment, 100 g of material was released from a funnel held 3.5 cm over a circular platform (Av diameter = 12 cm). The height of the cone was measured, and the angle of repose calculated using Equation 5 (Al-Hashemi and Al-Amoudi, 2018). Where material did not release freely from the funnel, material was lightly agitated. If the height of the cone reached the base of the

funnel, then the funnel was incrementally moved vertically to accommodate the growing cone. This was repeated three times for each experiment.

$$SAoR\ (°) = tan^{-1}\frac{2h}{D} \quad [6]$$

h = height (mm)

D = base diameter (mm)

Dynamic Angle of Repose (DAoR) was determined by rotating 100 g of material in a clear cylindrical drum at a constant rate (Smith, 2020). This was recorded on video and critical angle (the maximum angle prior to collapse) measurements analyzed using ImageJ (Schneider et al., 2012). This was completed three times.

Fluidisation Behaviour Tests

Experiments to determine the fluidisation behaviours of the volcanic material with increasing moisture contents were completed using a rectangular, near-2D fluidisation chamber with a porous base (following Gilbertson et al., 2020). Material (200.0 g) was measured, a weight % of water was added, and the homogeneous sample was then placed into the chamber and carefully levelled. A manometer probe recorded basal pore pressure changes during each experiment. Gas velocity (L/min) was increased incrementally until either a stable, channelised bubbling fluidisation state was achieved, or large amounts of winnowing or pressure build-up occurred. To limit the effects of drying from basal air flow, experiments were carried out with gradual increases in gas flow rate (0.8 – 3.00 L/min/min for dry sediments and 6.80 – 11.00 L/min/min for moisture added sediments) over a period of 01:11 – 23:51 minutes.

Results

Particle Size Analysis

The experiments were completed using volcanic material (V1 – V6). All samples are moderately to very well sorted (Fig. 2). Samples V1, V4, V5 and V6 were sieved into desired particle size distributions, whereas samples V2 and V3 were kept as natural volcanic particle size distributions (ranging from >74 - 300 µm). Particle size and sorting characterisation of each sample is presented in Table 3. As highlighted above, all samples fall into groups A and B of Geldart's classification, indicating that they should display excellent to fair flowability (Geldart, 1973).

Table 3 Table showing particle size mean (logarithmic), particle size median (log), particle range, fines content, geometric mean, logarithmic (Φ) Method of Moments used for Mean, Sorting, Skewness, and Kurtosis. Sauter mean diameter calculated from Breard et al (2019). Geldart Group (1973) based on size of particle.

Material	**Particle Size Mean ($\bar{x}$) ∅**	**Particle Size Median ∅**	**Particle Size Range (µm)**	**Fines Content (%)**	**Sorting Index (σ) ∅**	**Sorting (σ_G)**	**Skewness (Sk) ∅**	**Kurtosis (K) ∅**	**Sauter Mean (mm)**	**Geometric Mean (µm)**	**Geldart Group**
V1	3.776	3.734	2.5 – 297.3	35.76	0.428	Well	1.891	17.00	0.07	72.93	A
V2	3.215	3.320	15 - 425	21.41	0.710	Moderate	-0.524	2.576	0.11	107.5	A, B
V3	3.118	3.140	5 - 1000	19.57	0.868	Moderate	-0.562	4.140	0.12	115.0	A, B
V4	2.703	2.710	20 – 650	0.19	0.252	Very well	0.141	8.536	0.15	153.5	A, B
V5	1.508	1.568	10 – 1000	0.11	0.758	Moderate	- 0.103	2.480	0.42	347.3	A, B
V6	0.833	0.812	10 - 1000	0.05	0.445	Well	0.589	8.277	0.73	557.1	A, B

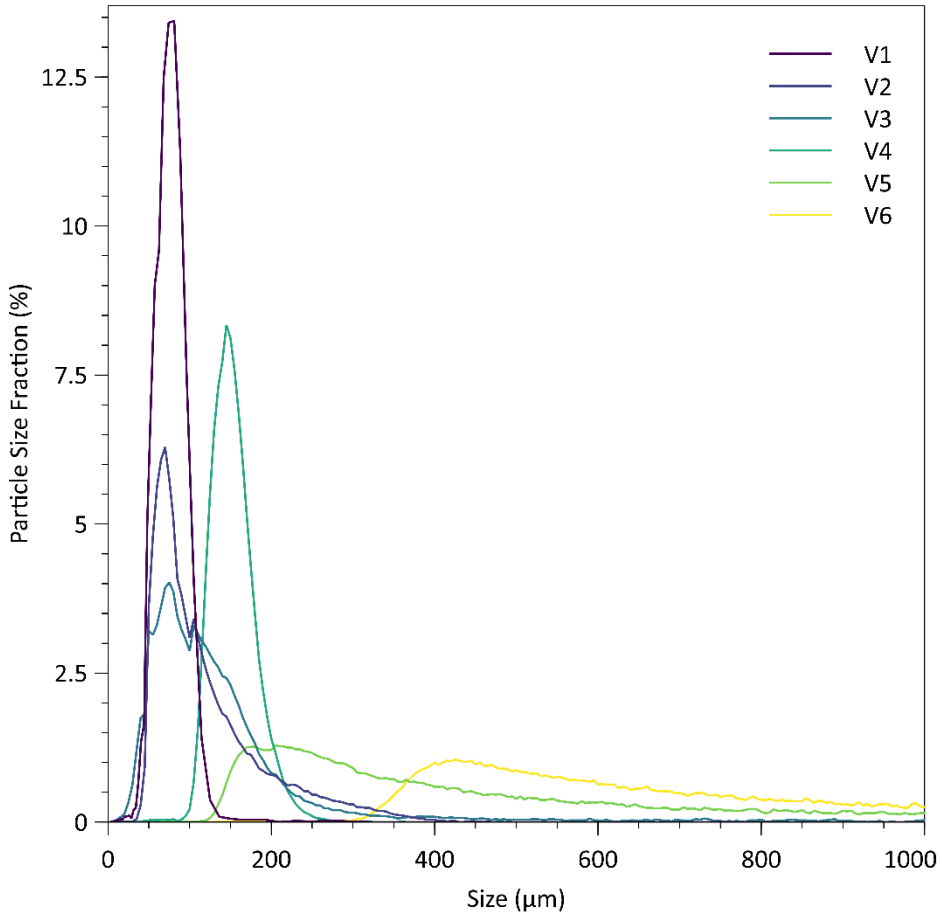

Fig. 2 Particle size analysis of volcanic material.

Bulk/Tapped Density

Table 4 Loose and tapped bulk density, the Hausner ratio, Carr Index and Flowability.

Material	Loose Bulk Density (kg m^{-3})	Tapped Bulk Density (kg m^{-3})	Hausner Ratio	Carr Index	Flowability
V1	*1310*	*1420*	*1.08*	*7.73*	Excellent
V2	*1320*	*1550*	*1.18*	*15.13*	Good
V3	*1380*	*1610*	*1.17*	*14.28*	Good
V4	*1320*	*1420*	*1.07*	*6.59*	Excellent
V5	*1280*	*1440*	*1.12*	*10.68*	Excellent

V6	*1180*	*1370*	*1.15*	*13.37*	Good

The bulk and tapped densities were calculated for volcanic samples ranging in sizes from finest (V1 – 3.8 ϕ) to coarsest (V6 – 0.8 ϕ). With increasing particle size, bulk and tapped densities generally decrease (Table 4). Material flowability, as determined by the Hausner Ratio and Carr Index, is good (V2, V3, V6) and excellent (V1, V4, V5) under the 0% moisture conditions. The change in flowability between V5 and V6 likely reflects the large increase in geometric mean from 347 (V5) to 557 (V6) (Table 3). V1, V4 and V5 all show excellent flowability, presumed to be related to the smaller particle range in V1 and V4 and having a low fines content in V5 (0.11%) (Table 3).

Angle of Repose

Static angle of repose (SAoR) increases with increasing across all volcanic samples (V1-6; Fig. 3). For the 0% moisture condition the SAoR ranges from 21° (V2, V4, V5) to 23° (V1, V3). Interestingly, these results show that under 0% moisture conditions, the SAoR is broadly similar (within 2°) regardless of particle size or sorting (Fig. 4a).

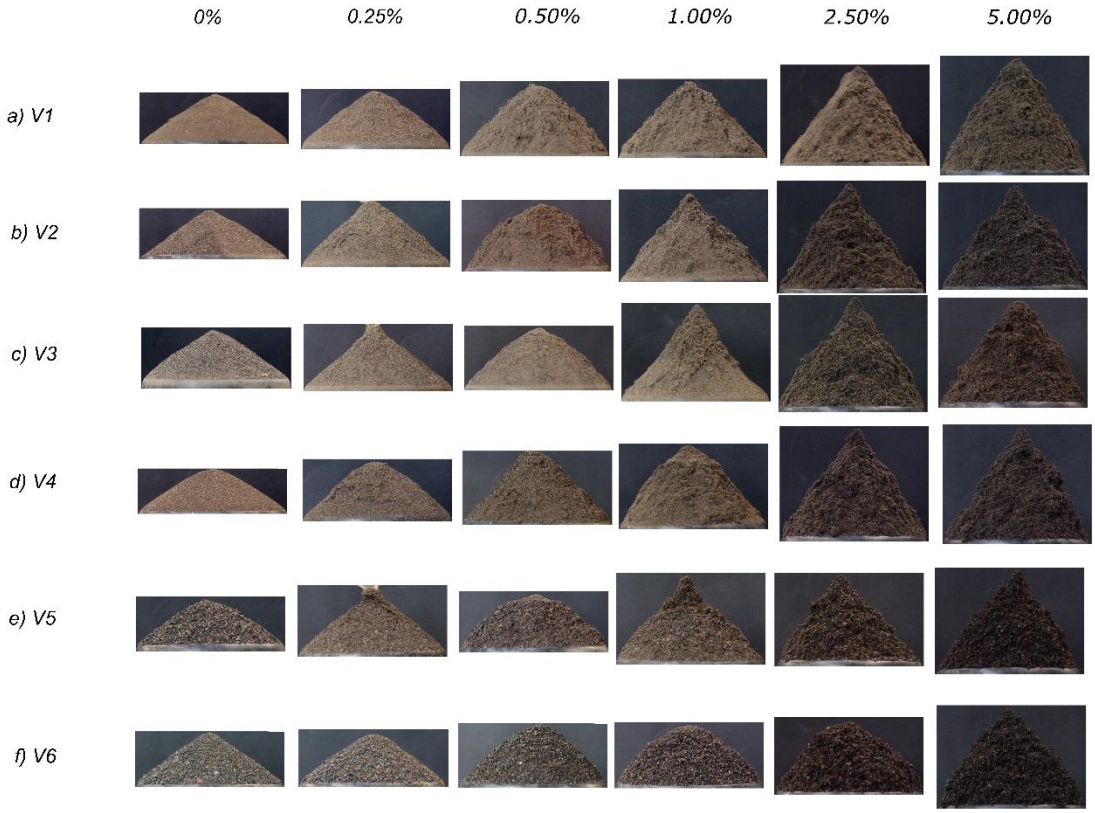

Fig. 3 Representative static angle of repose (SAoR) cone formation of V1 – V6.

When increasing moisture contents to 5% the SAoR values increase to approximately double those achieved with 0% moisture, approaching 42° (V5, V6) to 47° (V4). However, this relationship is not linear with increasing moisture content (Fig 4a). All materials show a rapid increase in SAoR with moisture to around 25°. However, beyond a moisture content of 0.5% a division is evident between the finer and course mixtures; those with Sauter mean diameters below 0.3 mm (V4, V3, V2) quickly increase to SAoR values of ~45° at moisture contents of 1-2 %, before plateauing and becoming invariant with additional moisture content. Mixtures with higher Sauter diameters (V1, V5, V6) show a more gradual increase in SAoR with moisture content. V5, with a Sauter mean diameter of 0.42 mm has somewhat intermediate behaviour, while V6 with a Sauter diameter of 0.73mm shows a more *linear* relationship for SAoR with moisture between 0.5 – 5%. This indicates that SAoR shows distinct sensitivity to increase in water in the materials and that relatively small weight percentages can produce very different cohesivities within the mixtures It is notable that fines-rich mixtures are particularly sensitive to moisture related cohesion, notably at <2 wt. %.

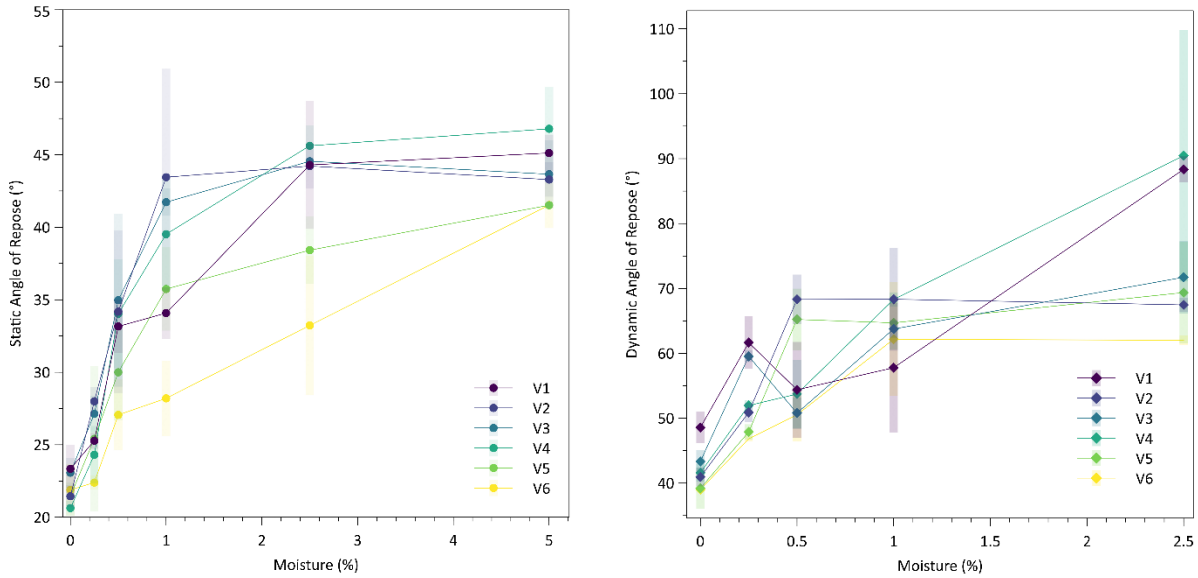

Fig. 4 a) SAoR for volcanic material with varying moisture percentages (0.00, 0.25, 0.50, 1.00, 2.50 and 5.00% with standard deviation error bars. b) DAoR critical angle of volcanic material with varying moisture percentages (0.00, 0.25, 0.50, 1.00 and 2.50%).

Figure 4 also shows the relationship pf Dynamic Angle of Repose experiments (Fig 4b). Generally, and similar to the SAoR result, there is an increase in the DAoR with increasing moisture. However, in experiments with increasing moisture levels (> 2.50%) the material was observed to clump, slide, and stick to the outer walls of the drum, complicating the results. Nonetheless, it is important to observe that the Sauter mean relationships detected within the SAoR experiments are not replicated in the DAoR setting.

Fluidisation experiments

Fluidisation behaviours were described via sidewall video analysis of the fluidisation chamber. The visual observation of gas escape structures (i.e., bubbling, channeling, pocketing, explosive channeling, cracking (Fig. 5 a-e) and gas velocity measurements have been recorded at varying moisture levels (Fig. 6 a - f).

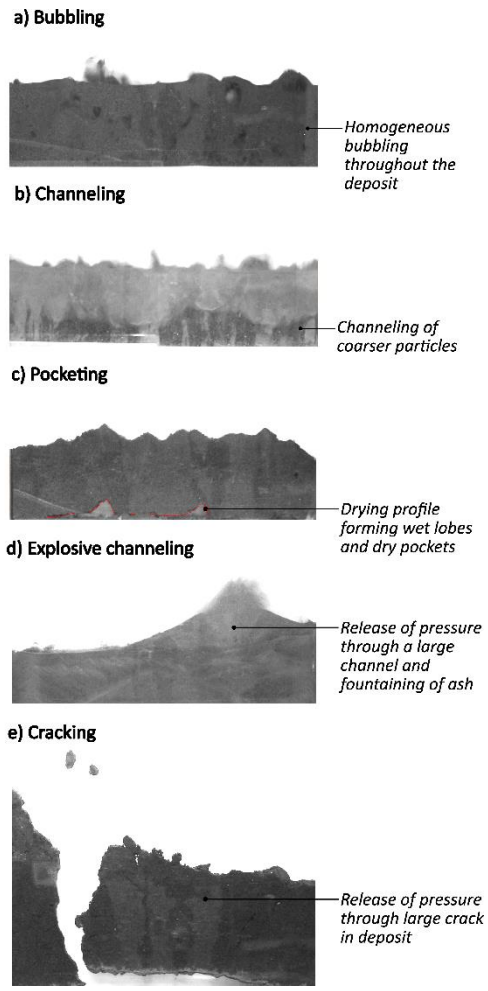

Fig. 5 a-e shows examples of the descriptive structures from across the experiments.

Bubbling gas escape (Fig. 5a) is seen initially in most experiments, where gas bubbles rise from the influx of gas within the deposit. With increasing gas flux, this can lead to channeling, where material is sorted through vertical channel or via pipe structures forming within the deposit (Fig. 5b). Drying profiles that migrate through the deposit are shown in Fig. 5c and as this migrates with non-uniformity in the vertical deposit, formation of areas of wet lobes and dry pockets can be observed (Fig. 5c). Where the material is dry and bubbling, this is referred to as pocketing. Explosive channeling can also be observed in some experiments (Fig. 5d), as the material dries, the upper wet deposit inhibits gas escape and causes a pressure increase and the subsequent release (Online Resource 1). Finally, under the highest moisture contents, material does not form any of the previous gas escape structures outlined above, instead, pressure builds until the deposit fractures into cracks where gas can easily permeate through (Fig. 5e; Online Resource 2).

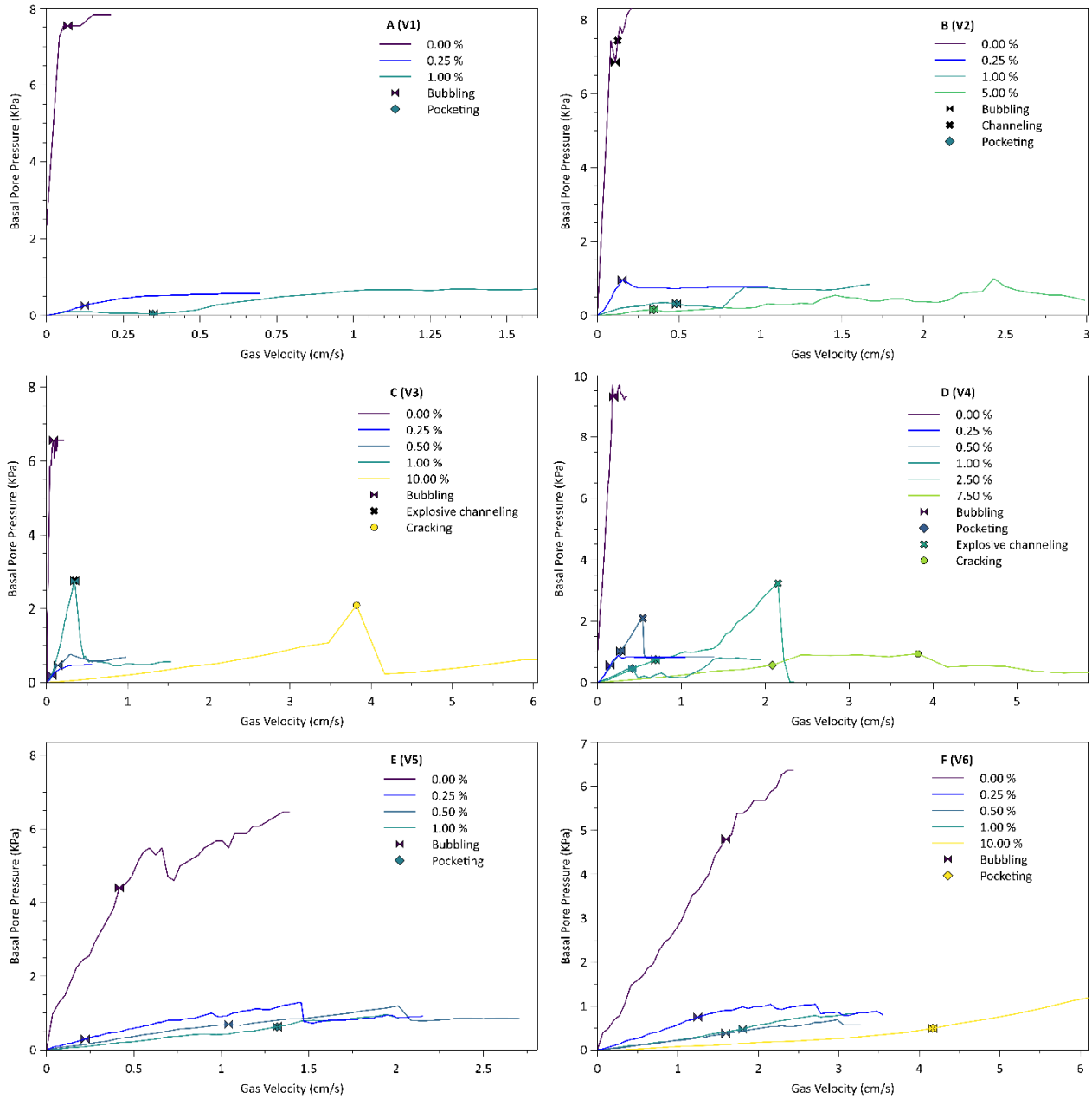

Fig. 6 A-F. Fluidisation profiles of V1 – V6 with increasing moisture (0.00 – 10.00 %). Symbols show gas escape structure formation.

0.00% Moisture

At 0.00% moisture for samples with moderate sorting (i.e., V2, V3, V5), fine material escapes through gas escape channels (Fig. 5b) in the lower area of the deposit. The observation of minimum bubbling (U_{mb}) is first seen in the upper fine fraction of the deposit at U_{mb} 0.11 (V2), 0.08 (V3), and 0.42 (V5) cm/s. There is often a separation of fines bubbling in the upper layer, a mid-area of coarse channeling (U_{mc}) at 0.13 (V2) and 0.10 (V3) cm/s as fines are being elutriated, and a coarse material layer at the base of the deposit. Bubbling only affects the finer material.

In volcanic mixtures that are well to very well sorted (i.e., V1, V4) bubbles rise uniformly throughout the whole deposit with a U_{mb} of 0.07 (V1) and 0.19 (V4) cm/s. Within the more coarse, well sorted, material (V6) bubbles

in a sluggish motion from the base of the deposit, with mostly bubbling (U_{mb} 1.60 cm/s) occurring in the upper half of the deposit and channeling in the lower. This reflects the slight particle size variation of material used, and therefore the Umb of the coarser material (Fig. 5b).

0.25% Moisture

At 0.25% moisture contents, similar behaviours are observed for V3 (U_{mb} 0.069 cm/s), V5 (U_{mb} 0.22 cm/s) and V6 (U_{mb} 1.25 cm/s) as described for 0.00% moisture. For V2 (U_{mb} 0.15 cm/s), V1 (U_{mb} 0.13 cm/s) and V4 (U_{mb} 0.15 cm/s), bubbling begins at the base of the deposit. However, as the surrounding wet deposit begins to dry, this dry material becomes incorporated into the bubbling deposit. In V2, we again see a separation of channeling and bubbling in the lower and upper deposit.

0.50% Moisture

At 0.50% moisture, a drying profile can be observed throughout most of the deposit (V4, V5, V6). In the V4 sample, as drying at the base moves throughout the deposit, dry material begins to bubble (U_{mb} 0.28 cm/s), and pressure slowly increases. This is released suddenly (explosive channeling) at 0.54 cm/s through a large channel which cuts through the moist, upper part of the deposit. As the surrounding wet material then begins to dry, it then becomes incorporated into the bubbling deposit. In the V5 sample, the drying profile forms lobes of wet material and pockets of dry material. The dry pockets slowly grow until reaching the upper deposit and begin to bubble (U_{mb} 1.04 cm/s). With continued drying as the experiment progresses, similar behaviours to the 0.25% and 0.00 % moisture levels experiments are observed. After the drying profile has moved through the deposit of V6, similar behaviours to 0.25% and 0.00% moisture levels are observed (U_{mb} 1.60 cm/s).

For the V3 material, channels of coarser material begin to slowly move towards the surface. Material begins to dry and is then incorporated into the bubbling deposit (U_{mb} 0.14 (V3).

1.00% Moisture

At 1.00% moisture, V1, V2, and V4 show material at the base of the deposit drying in pockets. The dry material begins to bubble (U_{mb} 0.35 (V1), 0.49 (V2), 0.42 (V4) cm/s) and as the surrounding wet material begins to dry, it is incorporated into the bubbling deposit. In V5 and V6, a distinctive drying profile moves throughout the deposit. Again, this creates dry pockets of bubbling material (U_{mb} 1.32 (V5), 1.81 (V6) cm/s) and wet lobes. In V3, pressure slowly builds as gas velocity is increased. Pressure is suddenly released through the formation of an explosive channel (0.35 cm/s). The dry deposit then begins to bubble (U_{mb} 0.35 cm/s) and is slowly incorporated into the surrounding drying material.

2.50% Moisture

At 2.50%, behaviours of V4 show similar results to 1.00% moisture content: as the base dries, bubbling pockets are formed (U_{mb} 0.70 cm/s) in-between lobes of wet material. In V4, pressure builds until it is suddenly released through an explosive channel (2.15 cm/s).

5.00% Moisture

At 5.00% V2 shows the deposit drying at the base which forms drying and bubbling (U_{mb} 0.35 cm/s) in pockets, and wet lobes.

7.50% Moisture

At 7.50%, a clear drying profile forms through the V4 deposit, cracks begin to form and move through the deposit until reaching the top and collapsing into pieces (3.82 cm/s). As gas was moving through cracks, there was no dramatic rise and release in pressure.

10.00% Moisture

Finally, at 10.00%, V3 forms a clear drying profile within the deposit. Pressure builds before being released suddenly at 3.82 cm/s. This forms a large crack in-between wet material. V6 shows a clear drying profile, as pressure slowly rises as small pockets eventually form and dry material begins to bubble (4.17 cm/s).

Key Observations

These fluidisation experiments clearly demonstrate how small additions of water into pyroclastic material can greatly impact fluidisation behaviours and resulting gas escape structures of a defluidising volcanic deposit. Two key observations are apparent in the experiments: 1) the drying profile, and 2) pressure build up and release.

The dynamics of the drying profile, as the moisture content is impacted by the fluidising gas, exert a strong control on the distribution of gas escape features, with variations across the grain size of the materials.

As gas flux is increased, a drying profile can move from the base to the top of the deposit. The drying profile forms more easily within the coarser materials (V3 – V6). The profile initially rises uniformly across the bed, before becoming irregular as it reaches the top of the deposit. These profiles are noted as they highlight vertical and lateral moisture heterogeneity within the deposit and their irregular structure determines the formation of drying pockets and wet lobes (Fig 5c). At low moisture percentages (< 2.50%) the drying pockets bubble and the wet lobes begin to dry before being incorporated into the pockets. However, at high moisture contents (> 2.5%) moisture rich lobes remain throughout the experiment, even at high gas velocities. This shows that within a defluidising deposit, a drying profile will lead to lateral and vertical variations in moisture.

In experiments with moisture contents of 0.50 – 10.00%, explosive channelling (V3, V4) and cracking (V3, V4) can occur. Across the experiments with 0.50 – 5.00% moisture contents, a wet impermeable cap was observed to form above the drier underlying deposits, with progressive drying of the vertical profile. Pressure builds under the cohesive cap and continues to rise with increasing gas velocity. This eventually results in explosive channeling and a sudden basal pressure drop as the overburden pressure is exceeded. In higher moisture levels (5.00 - 10.00%) experiments, the deposit does not dry as a relatively uniform rising profile. Instead, pressure builds as the gas velocity is increased until cracks form in the deposit. These cracks act as effective gas escapes and release the pore pressure.

Discussion

The impact of moisture on ignimbrite material and PDC behaviour is relatively understudied, with previous detailed investigations having traditionally focused on dry (Wilson, 1980) and saturated (Roche et al., 2001) extremes. However, direct observations have shown that variable amounts of moisture can enter a PDC system (Cole et al., 1998, 2002; Lipman, 2019; Vecino et al., 2022) and accretionary lapilli and ash pellets are believed to provide evidence for the presence of moisture within PDCs (Branney and Kokelaar, 2002; Brown and Branney, 2004; Druitt, 2014). Our results show that with increasing moisture content: 1) the cohesivity of ignimbrite material alters drastically, even with very small weight-percent amounts (> 0.50%); 2) an increase in moisture can change flow property behaviours from a free flowing to a non-flowing material; 3) changes in moisture affects fluidisation profiles and gas escape structures; 4) a defluidising deposit can lead to a drying profile, and therefore lateral and vertical heterogeneity within the deposit; and 5) pressure can increase where gas escape is hindered by moisture, which can cause dramatic releases of pressure in an explosive fashion. Here we discuss the implications of these findings for the flow behaviour of a PDC and variations in deposit sedimentology and broader architecture.

Material Behaviours

These experiments show that in a dry (0%) sample, material with a grainsize of 5 – 1000 μm has low cohesivity. The cohesive nature of dry material heavily depends on the fine ash content of the material. For example, angle of repose is highest in samples V1 and V3 which have some of the highest % of fines (Table 3.1). However, results indicate that sorting plays a key role; V5 has one of the lowest fines contents (0.11 %) but has the same SAoR value as V2 which has a high fines content of 21.41 %. V2 and V5 have a large size range, similar sorting indexes (V2 – 0.710, V5 – 0.758 ϕ) and the lowest kurtosis values (V2 – 2.58, V5 – 2.48 ϕ). When dry, all samples have good flowability and are said to be free flowing (i.e., when fluidised the deposit demonstrates bubbling and channeling throughout the deposit). Results from the Bulk/Tapped density experiments show that V1 and V4 exhibit some of the best flowing behaviors. V1 is well sorted and displays the largest volumes of fines (35.76%) whereas V4 is very well sorted and has one of the lowest volumes of fine material (0.11%). The excellent flowability seen in V4 may result from its sorting and resulting packing behaviour, which is known to affect flow behaviour (Breard et al., 2023). The DAoR results show contrasting behaviours versus the SAoR results when comparing against the Sauter mean diameter. This suggests that particle size controls are likely to be more important in understanding the remobilisation of static deposits than in the flowability of particles already in motion.

Such an observation has wide ranging implications. For example, Breard et al (2023) suggests that long run-out distances in block and ash flows (BAFs) were a result of large degrees of fragmentation, with the current becoming more fines rich, and subsequently the deposit displaying higher packing. These particle size changes result in a dynamically evolving flow where fines formation and increasing packing behaviour reflect elevated pore-pressure within the flow (Breard et al., 2023). Our experiments (V1, V4) show that both fines content and packing can contribute to good flowability behaviours, with implications for run-out distances.

The material with the larger volume of fines (V1, V2) is shown to exhibit more cohesive behaviours with increasing moisture (i.e., higher SAoR angle). V4, which is more well sorted, has the highest increase in SAoR values. Our work demonstrates how important the role of moisture can be, at small amounts, in changing flowability behaviours. We can build a hypothesis that the addition of moisture into a PDC during propagation, with increasing fragmentation and packing, can be a factor in controlling run-out distances – higher moisture contents reduce flowability so may reduce maximum runout distances, particularly in flows with enhanced fragmentation.

We can then assume that during deposition from a PDC the fine ash fraction of a deposit, and material with increased packing, may be more influenced by water – and therefore hold a higher moisture content during deposition. Within a material with >30% volume of fines, the stress forces begin to be dominated by the fine fraction (Li et al., 2020; Breard et al., 2023). A large volume of fines, both with and without moisture, may dramatically alter the deposition and the preservation potential of these layers. This has implications for understanding deposit architecture behaviours (e.g., gas escape structures) or extents (e.g., erosion of ash-rich layers).

Gas Escape Structures

A variety of gas escape structures were observed in the fluidisation experiments, with many related to moisture content. Here we define three main types of behaviour (Table 5). In Type 1 (0.00 - < 0.50%) we see partial fluidisation and segregation of heterogenous material through bubbling and channeling. In material with a smaller size range, small vertical bubbling occurs across the entirety of the deposit. During Type 2 (0.50 – 5.00%), an irregular drying profile develops and moves through the deposit from the base. As the drying profile grows, dry pockets of bubbling material begin to form in between irregular lobes of wet material. Explosive channeling also occurs, which releases pressure and facilitates quicker drying of the whole deposit. Finally, during Type 3 (7.50 – 10.00%), similar lobe and pocket structures are formed to Type 2 but are accompanied by cracking processes, where fractures in the wet material form to accommodate rapid gas escape.

Table 5 Varying types of behaviour of gas escape observed with increasing moisture in volcanic material.

	Type 1	Type 2	Type 3
Moisture Range	0.00 – 0.25%	0.50 – 5.00%	7.50, 10.00%
Bubbling	Yes	Yes	Yes
Channeling	Yes	Yes	No
Drying Profile	No	Yes	Yes

Pocketing	No	Yes	Yes
Explosive Channeling	No	Yes	No
Cracking	No	No	Yes

Roche et al., (2001) investigated the water fluidisation behaviour of ignimbrite material where material was saturated and subjected to an increase in fluid velocity. Similarly, the findings of Wilson (1980; 1984) and the experiments herein demonstrate gas escape structures forming from aggregative behaviour. The gas escape structures were all fines depleted and rich in dense and coarse material. However, the aqueous gas escape structures (pipes) were observed to form at lower fluid velocities than the aerated structures (Fig. 7).

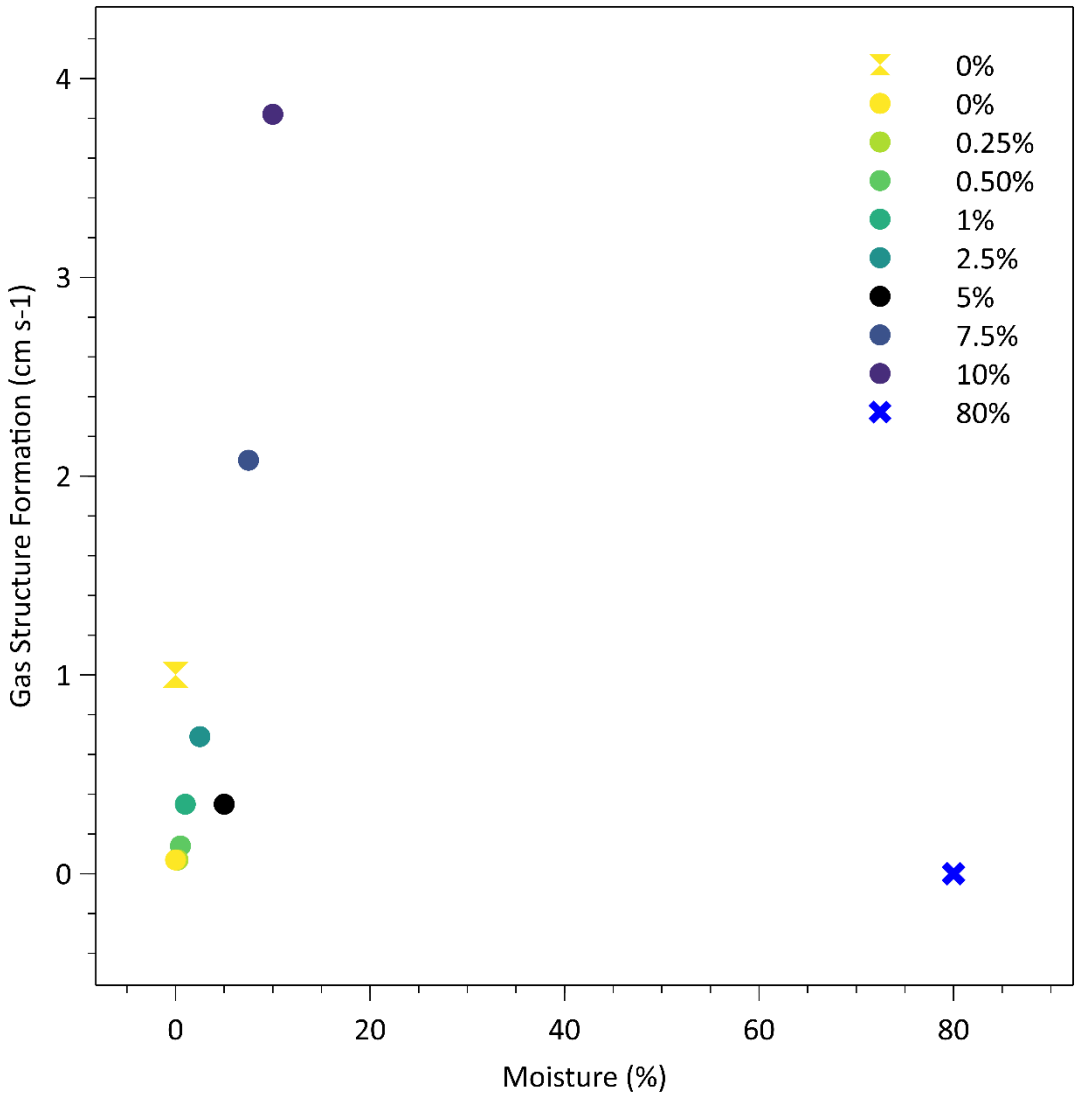

Fig.7 showing minimum gas velocity of gas escape structure formation for dry, moisture-influenced, and saturated deposits. Wilson (1980) values (hourglass) based on first formation of pipes (0% wt.). The values of our results (circles) are from first formation of gas escape structure seen in V1-V6 at varying moisture

percentages (i.e., bubbling at lower %'s, explosive cracking at the highest %'s). Roche et al., (2001) values (cross) are on initial pipe formation (80% wt.).

Figure 7 shows that by increasing moisture within a sample, higher gas velocities are required for aggregative fluidisation. However, between 10 and 80% moisture there is a change in the dominant fluidising medium, from gas to water. Instead of impeding early fluidisation structures, a large increase in moisture leads to more regular structures forming. This can be explained by changing particle-water states with increasing moisture. Aggregative fluidisation mechanisms will result in the segregation of particles through gas escape structures, where fines are winnowed. The nature of segregation will depend on the particle concentration and the size, shape, density, and relative proportions of clasts (Sparks, 1976; Wilson, 1980; 1984; Branney and Kokelaar, 2002). We find that the moisture content of the deposit also controls this process; segregation structures can change dynamically with drying or become hindered with increasing moisture influence. This is due to our material being in a predominantly capillary state (Kim and Hwang., 2003; Kim and Sture, 2008). At higher levels of moisture, particles reach a more saturated state, are completely supported by capillary bonds and fluidisation behaviours are no longer inhibited (as seen in Roche et al., 2001; Kim and Hwang., 2003). We observe that even small influences of moisture (as low as 0.50% by weight) into volcanic material may control the formation and nature of gas escape structures.

Application to natural deposits

Our results show introducing moisture into volcanic materials may cause changes in gas escape morphology. Gas escape structures have been recorded and described extensively within field volcanological literature (e.g. Fisher and Schmincke, 1984; Pacheco-Hoyos et al., 2020). They have been described as pods and pipes displaying single or branching patterns, or as lenticular, curvilinear, and crescentic shaped (Wilson, 1980; Branney and Kokelaar, 2002; Pacheco-Hoyos et al., 2020). They can be spatially arranged within individual layers or can move through multiple layers and are often fines depleted. Our results demonstrate varied morphologies, including vertical channels, sub-vertical cracks, and pods (created by moisture-rich lobes and dry pockets).

Changes in gas escape structures in ignimbrites are thought to be dominated by heterogeneity within ignimbrite material (e.g., size, density, shape etc.; Wilson, 1984; Pacheco-Hoyos et al., 2020). We propose that varying moisture levels will also influence changes in gas escape morphology and may explain circumstances where morphological changes are observed when other conditions appear unchanged. More detailed documentation of morphology of field examples may allow for improved interpretations of depositional environment.

Morphological changes in gas escape structures also have implications for drying profiles and resulting heterogeneities within a deposit. In our experiments, the formation of a drying profile demonstrates both vertical and lateral variation due to an undulating contact between wet and dry material resulting in vertical and lateral changes in the tensile strength of a deposit. This may have implications for erodibility, remobilisation (as well as preservation potential), and subsequent deposition of certain layers within a deposit.

Mechanism for secondary eruptions

Secondary eruptions in ignimbrite deposits form due to the interaction between water and hot material (Van Westen and Daag, 2005). When in contact with a hot ignimbrite, steam will expand and cause sudden explosive decompression. Secondary eruptions form large craters (20 – 80m depth), can remobilize large volumes of ignimbrite material and can occur for years after the initial eruption (the 1991 Mount Pinatubo generated secondary eruptions for up to a year; Riehle et al., 1995; Van Westen and Daag, 2005). Riehle et al., (1995) modelled cooling, degassing and compaction behaviours within ignimbrites. High temperatures were most likely to remain elevated within deposits >50 m thick, with temperatures cooling mostly by groundwater and some influence from rainfall. Keating et al (2005) modelled that the addition of water on a hot deposit can result in exceeded pore pressure, in turn exceeding the overburden pressure. This can result in secondary eruptions.

Moyer and Swanson (1987) described three styles of secondary eruptions - passive degassing (least explosive), ash fountaining and explosive cratering (most explosive) - controlled by thermal energy and the permeability of the overlying material. Analogue experiments investigating the mechanisms of secondary hydroeruptions have been explored by Gilbertson et al (2020). They identified that vertical changes in size fractions, and therefore a vertical profile of minimum fluidisation velocities, resulted in secondary hydroeruptions. In these experiments, a deposit capped with coarser material formed an upward doming bed leading to an explosive release of material. This was due to a drag-induced system. The fine-particle layer below acted as a lower minimum fluidisation layer that was unable to fluidise the overlying, coarser layer, resulting in pressure increase and release.

Secondary eruptions are associated with subaerial PDC deposits, and also with sub-aqueous PDCs (Krakatau, 1883; Mandeville et al., 1996) and sub-marine sediments (Hovland et al., 2002; Rogers, 2015; Cojean et al., 2021) and Martian impact craters (Boyce et al., 2012). Martian pits in impact craters are thought to be formed by water loss from exsolving vaporizing water, creating streams of gas and the funneling out of fine ejecta towards the surface (Boyce et al., 2012). Pockmarks are circular craters that form in the sub-aqueous environment: deep marine, lakes, lacustrine (Cojean et al., 2021). They can form from the upward movement of fluid (liquid or gas), the trapping of the fluid by an impermeable cap, or from gradual accumulation of the fluid until the gas is released. The fine mud particles within these environments can be extremely cohesive, and therefore display a very high tensile strength, which is what can form the impermeable overburden material in these environments (Rogers, 2015). Pockmarks have also been known to form in association with slides and slumps (Hovland et al., 2002).

Analogous to all the mechanisms for secondary hydroeruptions is an active moving pore pressure (i.e., vaporization in meteorites) as well as a vertical variation in the permeability of a material (i.e., fine, or mud-rich material, minimum fluidisation velocities). Results from our experiments show that increasing moisture levels within the fluidised deposit can lead to impermeable layers forming through drying. By increasing moisture throughout our experiments, we exhibit passive degassing (0%), ash fountaining (> 0.50% wt.) and

explosive cratering (> 0.50% wt.) behaviours as described in Moyer and Swanson (1987). After lithostatic pressure of the impermeable wet cap is overcome, explosive channeling (> 0.50% wt.) and cracking (> 7.50% wt.) occurs (named *explosive cratering* by Moyer and Swanson., 1987). Similarly, to these works, our results herein demonstrate the impact of intermediate permeability on secondary eruptive styles. We argue that the change from passive degassing to explosive cratering is not only a reflection of thermal energy in the system (as our material cooled significantly throughout the length of experiment), but also by internal degassing of a partially fluidised deposit.

Critically, our results suggest a potential new mechanism for secondary eruptions that form in a moisture influenced material (Fig. 8a). In our experiments, the addition of water during deposition results in increased cohesion and resulting tensile strength. As the deposit dries from the base, we see a shift in gas escape as the material begins to dry and bubble. In our model (Fig. 8a), the upper moisture rich layer inhibits passive de-gassing and leads to increased pore-pressure. With increasing pressure in the deposit, the overburden strength of wet material is compromised. The result is a sudden pressure release by explosive channeling and cracking, which mimics similar behaviours seen in secondary eruptions in ignimbrite deposits. Additionally, in a dry deposit later moistened by water (i.e., precipitation), the upper moisture-rich layers of material will create an overall denser material (Fig. 8b).

Application to field examples

Secondary eruptions were observed following the Mt St. Helens 1980 and Mt Pinatubo 1991 events (Keating, 2005) and were attributed to variations in the permeability of ignimbrite deposits caused by the presence of water (e.g., rainfall and lacustrine environments) (Moyer and Swanson, 1987; Manville et al., 2002). It is thought that high pressure towards the base of these ignimbrites, caused by vaporization of water, led to low-permeable layers preventing the balancing of pore pressures throughout the deposit, which resulted in explosive depressurization (Keating, 2005). Keating (2005) suggests that after emplacement, hydrological re-establishment may begin to occur and interaction with hot overlying ignimbrite material may result in the formation of secondary hydroeruptions.

Our moisture influenced model may provide an explanation for the observations of secondary eruptions in deposits that have aggraded with the presence of water (e.g., secondary eruptions followed the previous location of the Rogue River; Druitt and Bacon, 1986) (Fig. 8a) and that have interacted with rain (e.g., Mt Pinatubo, Daag and Westen, 1996) (Fig. 8b). Rainfall may create a moisture-rich cap to the deposit that is impermeable to degassing from the lower deposit. The increased moisture from the rain would result in an increased cohesivity, and therefore tensile strength, of the material. With gas escape inhibited, pressure may continue to build until the overburden pressure is reached, and degassing is then allowed to escape through a secondary eruption in the deposit.

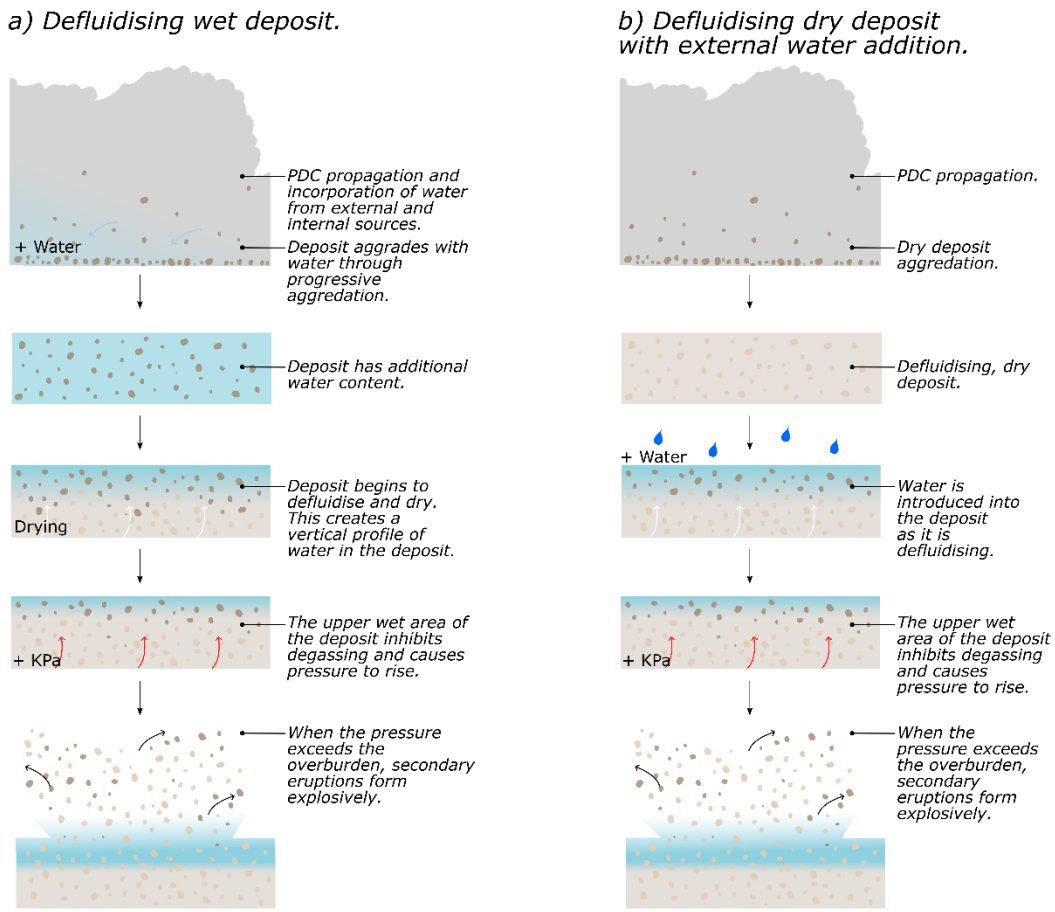

Fig. 8 moisture-influenced model of secondary eruption formation by a) a defluidising wet deposit and b) a defluidising dry deposit with external influences of water.

Conclusion

This work highlights the importance of moisture introduced into PDCs both in terms of PDC flow dynamics as well as the characteristics of the resultant deposits. Our results show that: 1) the cohesivity of ignimbrite material changes drastically, even though relatively small additions of moisture amounts (> 0.50%); 2) an increase in moisture can entirely alter flow property behaviour from a free flowing to a non-flowing material; 3) changes in moisture impact fluidisation profiles and gas escape structures; 4) a defluidising deposit can lead to a moisture profile, and therefore lateral and vertical heterogeneity within the deposit, and 5) pressure can increase where gas escape is hindered by cohesive substrates driven by moisture content, resulting in secondary eruptions. This builds on previous models of secondary eruptions in deposits and supports the idea that they are formed because of the development of an impermeable capping layer, here created by the addition of moisture. This work further proposes that moisture within a defluidising deposit profile may hinder or change the formation of gas escape structures, which can then also lead to pressure increase and release, with significant implications for the interpretations of the sedimentary structures within the deposits. Overall, the work has shown the critical role of moisture within PDC dynamics and the implications for the erodibility of a material, preservation potential and the broader understanding of deposit architecture.

Reference

Abdullah, E.C. and Geldart, D. (1999) 'The use of bulk density measurements as flowability indicators', *Powder Technology*, 102(2), pp. 151–165. Available at: https://doi.org/10.1016/S0032-5910(98)00208-3.

Amidon, G.E., Meyer, P.J. and Mudie, D.M. (2017) 'Particle, Powder, and Compact Characterization', in *Developing Solid Oral Dosage Forms*. Elsevier, pp. 271–293. Available at: https://doi.org/10.1016/B978-0-12-802447-8.00010-8.

Barclay, J., Johnstone, J.E. and Matthews, A.J. (2006) 'Meteorological monitoring of an active volcano: Implications for eruption prediction', *Journal of Volcanology and Geothermal Research*, 150(4), pp. 339–358. Available at: https://doi.org/10.1016/j.jvolgeores.2005.07.020.

Beakawi Al-Hashemi, H.M. and Baghabra Al-Amoudi, O.S. (2018) 'A review on the angle of repose of granular materials', *Powder Technology*, 330, pp. 397–417. Available at: https://doi.org/10.1016/j.powtec.2018.02.003.

Benage, M.C., Dufek, J. and Mothes, P.A. (2016) 'Quantifying entrainment in pyroclastic density currents from the Tungurahua eruption, Ecuador: Integrating field proxies with numerical simulations', *Geophysical Research Letters*, 43(13), pp. 6932–6941. Available at : https://doi.org/10.1002/2016GL069527.

Boyce, J.M. *et al.* (2012) 'Origin of small pits in Martian impact craters', *Icarus*, 221(1), pp. 262–275. doi: 10.1016/j.icarus.2012.07.027.

Branney, M. and Kokelaar, P. (2002) *Pyroclastic Density Currents and the Sedimentation of Ignimbrites*.

Branney, M.J. and Kokelaar, P. (1992) *A reappraisal of ignimbrite emplacement: progressive aggradation and changes from particulate to non-particulate flow during emplacement of high-grade ignimbrite*. Springer-Verlag, pp. 504–520.

Breard, E.C.P. *et al.* (2019) 'The Permeability of Volcanic Mixtures—Implications for Pyroclastic Currents', *Journal of Geophysical Research: Solid Earth*, 124(2), pp. 1343–1360. Available at: https://doi.org/10.1029/2018JB016544.

Breard, E.C.P. *et al.* (2023) 'The fragmentation-induced fluidisation of pyroclastic density currents', *Nature Communications*, 14(1), p. 2079. Available at : https://doi.org/10.1038/s41467-023-37867-1.

Brown, R.J. *et al.* (2010) 'Origin of accretionary lapilli within ground-hugging density currents: Evidence from pyroclastic couplets on Tenerife', *Bulletin of the Geological Society of America*, 122(1–2), pp. 305–320. Available at: https://doi.org/10.1130/B26449.1.

Brown, R.J., and Branney, M.J. (2013) 'Internal flow variations and diachronous sedimentation within extensive, sustained, density-stratified pyroclastic density currents flowing down gentle slopes, as revealed by the internal architectures of ignimbrites on Tenerife', *Bulletin of Volcanology*, 75(7), pp. 1–24. Available at: https://doi.org/10.1007/s00445-013-0727-0.

2014 The United States Pharmacopeial Convention (2015) *Bulk density and tapped density of powders - US pharmacopeia (USP), ⟨616⟩ Bulk Density and Tapped Density of Powders*. Available at: https://www.usp.org/sites/default/files/usp/document/harmonization/gen-chapter/bulk_density.pdf (Accessed: 02 June 2023).

Camuffo, D. (2019) 'Theoretical Grounds for Humidity', in *Microclimate for Cultural Heritage*. Elsevier, pp. 43–59. Available at: https://doi.org/10.1016/B978-0-444-64106-9.00003-1.

Cas, R.A., and Wright, J.V. (1991) 'Subaqueous pyroclastic flows and ignimbrites: an assessment', *Bulletin of Volcanology*, 53(5), pp. 357–380. Available at: https://doi.org/10.1007/BF00280227.

Chédeville, C. and Roche, O. (2015) 'Influence of slope angle on pore pressure generation and kinematics of pyroclastic flows: insights from laboratory experiments', *Bulletin of Volcanology*, 77(11), p. 96. Available at : https://doi.org/10.1007/s00445-015-0981-4.

Chen, D. *et al.* (2021) 'Critical Shear Stress for Erosion of Sand-Mud Mixtures and Pure Mud', *Frontiers in Marine Science*, 8. Available at: https://doi.org/10.3389/fmars.2021.713039.

Chigira, M. and Yokoyama, O. (2005) 'Weathering profile of non-welded ignimbrite and the water infiltration behaviour within it in relation to the generation of shallow landslides', *Engineering Geology*, 78(3–4), pp. 187–207. Available at: https://doi.org/10.1016/j.enggeo.2004.12.008.

Cocco, R., Reddy, S.B. and Knowlton, K.T. (2014) *Back to Basics Introduction to Fluidization*. Available at: www.aiche.org/cep.

Cojean, A.N.Y. *et al.* (2021) 'Morphology, Formation, and Activity of Three Different Pockmark Systems in Peri-Alpine Lake Thun, Switzerland', *Frontiers in Water*, 3, p. 666641. Available at: https://doi.org/10.3389/frwa.2021.666641.

Cole, P.D. *et al.* (1998) *Pyroclastic flows generated by gravitational instability of the 1996-97 Lava Dome of Soufriere Hills Volcano, Montserrat*, pp. 3425–3428. Available at: https://doi.org/10.1029/98GL01510.

Cole, P.D. *et al.* (2002) 'Deposits from dome-collapse and fountain-collapse pyroclastic flows at Soufriere Hills Volcano, Montserrat', *Geological Society*, 21, pp. 231–262.

Daag, A & Westen, C.J. (1996). Cartographic modelling of erosion in pyroclastic flow deposits of Mount Pinatubo, Philippines. ITC Journal. 2. 110-124.

Dartevelle, S. *et al.* (2002) 'Origin of the Mount Pinatubo climactic eruption cloud: Implications for volcanic hazards and atmospheric impacts', *Geology*, (7), p. 663.

Deb, P.K. *et al.* (2018) 'Particulate level properties and its implications on product performance and processing', *Dosage Form Design Parameters*, pp. 155–220. doi:10.1016/b978-0-12-814421-3.00005-1.

Druitt, T. H., Bruni, G., Lettieri, P., and Yates, J. G. (2004), The fluidization behaviour of ignimbrite at high temperature and with mechanical agitation, *Geophys. Res. Lett.*, 31, L02604, doi:10.1029/2003GL018593.

Druitt, T. & Avard, Geoffroy & Bruni, G. & Lettieri, Paola & Maez, F.. (2007). Gas retention in fine-grained pyroclastic flow materials at high temperatures. Bulletin of Volcanology. 69. 881-901. 10.1007/s00445-007-0116-7.

Druitt, T.H. (2014) 'New insights into the initiation and venting of the Bronze-Age eruption of Santorini (Greece), from component analysis', *Bulletin of Volcanology*, 76(2), p. 794. Available at: https://doi.org/10.1007/s00445-014-0794-x.

Druitt, T.H. and Bacon, C.R. (1986) 'Lithic breccia and ignimbrite erupted during the collapse of Crater Lake Caldera, Oregon', *Journal of Volcanology and Geothermal Research*, 29(1–4), pp. 1–32. Available at: https://doi.org/10.1016/0377-0273(86)90038-7.

Duane, W.J. *et al.* (2008) 'General characteristics of temperature and humidity variability on Kilimanjaro, Tanzania', *Arctic, Antarctic, and Alpine Research*, 40(2), pp. 323–334. Available at: https://doi.org/10.1657/1523-0430(06-127) [DUANE]2.0.CO;2.

Dufek, J. (2016) 'The Fluid Mechanics of Pyroclastic Density Currents', *Annual Review of Fluid Mechanics*, 48, pp. 459–485. Available at : https://doi.org/10.1146/annurev-fluid-122414-034252.

Eychenne, J. *et al.* (2012) 'Causes and consequences of bimodal grain-size distribution of tephra fall deposited during the August 2006 Tungurahua eruption (Ecuador)', *Bulletin of Volcanology*, 74(1), pp. 187–205. Available at: https://doi.org/10.1007/s00445-011-0517-5.

Fisher, R.V. and Schmincke, H.-U. (1984) 'Pyroclastic flow deposits', *Pyroclastic Rocks*, pp. 186–230. doi:10.1007/978-3-642-74864-6_8.

Geldart, D. (1973) *Elsevier Sequoia SA, Lausanne-Printed in the Netheriands Types of Gas Fluidization*, *Powder Technology*, pp. 285–292.

Gilberston, M.A. *et al.* (2020) 'A Fluidisation Mechanism for Secondary Hydroeruptions in Pyroclastic Flow Deposits', *Frontiers in Earth Science*, 8. Available at: https://doi.org/10.3389/feart.2020.00324.

Girolami, Laurence & Druitt, T. & Roche, Olivier & Khrabrykh, Z.V. (2008). Propagation and hindered settling of laboratory ash flows - art. no. B02202. Journal of Geophysical Research. 113. 10.1029/2007JB005074.

L. Girolami, T.H. Druitt, O. Roche. (2005). Towards a quantitative understanding of pyroclastic flows: Effects of expansion on the dynamics of laboratory fluidized granular flows, Journal of Volcanology and Geothermal Research, Volume 296, Pages 31-39, ISSN 0377-0273, https://doi.org/10.1016/j.jvolgeores.2015.03.008.

G.Giordano, Ray A.F. Cas. (2021). Classification of ignimbrites and their eruptions, Earth-Science Reviews, Volume 220, https://doi.org/10.1016/j.earscirev.2021.103697

Gorle, A.P. and Chopade, S.S. (2020) 'Liquisolid Technology: Preparation, Characterization and Applications', *Journal of Drug Delivery and Therapeutics*, 10(3-s), pp. 295–307. Available at: https://doi.org/10.22270/jddt.v10i3-s.4067.

Hartmann, D.L. (2016). *Global physical climatology* (Vol. 103). Newnes.

Hausner, H.H. (1981) 'Powder characteristics and their effect on powder processing', *Powder Technology*, 30(1), pp. 3–8. Available at: https://doi.org/10.1016/0032-5910(81)85021-8.

Hovland, M., Gardner, J.V. and Judd, A.G. (2002) 'The significance of pockmarks to understanding fluid flow processes and geohazards', *Geofluids*, 2(2), pp. 127–136. Available at: https://doi.org/10.1046/j.1468-8123.2002.00028.x.

Houghton, B., White, J.D.L. and Van Eaton, A.R. (2015) 'Phreatomagmatic and Related Eruption Styles', in *The Encyclopaedia of Volcanoes*. Elsevier, pp. 537–552. Available at: https://doi.org/10.1016/B978-0-12-385938-9.00030-4.

Hurwitz, S. (2003) 'Groundwater flow, heat transport, and water table position within volcanic edifices: Implications for volcanic processes in the Cascade Range', *Journal of Geophysical Research*, 108(B12). Available at: https://doi.org/10.1029/2003jb002565.

Keating, G.N. (2005) 'The role of water in cooling ignimbrites', *Journal of Volcanology and Geothermal Research*, 142(1-2 SPEC. ISS.), pp. 145–171. Available at: https://doi.org/10.1016/j.jvolgeores.2004.10.019.

Kim, T.-H. and Hwang, C. (2003) 'Modelling of tensile strength on moist granular earth material at low water content', *Engineering Geology*, 69(3–4), pp. 233–244. doi:10.1016/s0013-7952(02)00284-3.

Kim, T.-H. and Sture, S. (2008) 'Capillary-induced tensile strength in unsaturated sands', *Canadian Geotechnical Journal*, 45(5), pp. 726–737. Available at: https://doi.org/10.1139/T08-017.

LaMarche, C.Q. *et al.* (2016) 'Linking micro-scale predictions of capillary forces to macro-scale fluidization experiments in humid environments', *AIChE Journal*, 62(10), pp. 3585–3597. Available at: https://doi.org/10.1002/aic.15281.

Leturia, M. *et al.* (2014) 'Characterization of flow properties of cohesive powders: A comparative study of traditional and new testing methods', *Powder Technology*, 253, pp. 406–423. Available at: https://doi.org/10.1016/j.powtec.2013.11.045.

Li, W.C. *et al.* (2020) 'Effects of stress state and fine fraction on stress transmission in internally unstable granular mixtures investigated via discrete element method', *Powder Technology*, 367, pp. 659–670. Available at: https://doi.org/10.1016/j.powtec.2020.04.024.

Lipman, P.W. (2019) 'When ignimbrite meets water: Mega scale gas-escape structures formed during welding', *Geology*, 47(1), pp. 63–66. Available at: https://doi.org/10.1130/G45772.1.

Ludwig, B., Millington-Smith, D., Dattani, R., Adair, J. H., Posatko, E. P., Mawby, L. M., Ward, S. K., & Sills, C. A. (2020). Evaluation of the hydrodynamic behaviour of powders of varying cohesivity in a fluidized bed using the FT4 Powder Rheometer®. *Powder Technology*, *371*, 106–114. https://doi.org/10.1016/j.powtec.2020.05.042

Ma, Y. *et al.* (2019) 'Modelling the effect of moisture on the flowability of a granular material', *Meccanica*, 54(4–5), pp. 667–681. Available at: https://doi.org/10.1007/s11012-018-0901-8.

Manville, V., Segschneider, B. and White, J.D.L. (2002) 'Hydrodynamic behaviour of Taupo 1800a pumice: implications for the sedimentology of remobilized pyroclasts', *Sedimentology*, 49(5), pp. 955–976. Available at: https://doi.org/10.1046/j.1365-3091.2002.00485.x.

Matthews, A.J., Barclay, J. and Johnstone, J.E. (2009) 'The fast response of volcano-seismic activity to intense precipitation: Triggering of primary volcanic activity by rainfall at Soufrière Hills Volcano, Montserrat', *Journal of Volcanology and Geothermal Research*, 184(3–4), pp. 405–415. Available at: https://doi.org/10.1016/j.jvolgeores.2009.05.010.

Moondra, S. *et al.* (2018) 'Bulk Level Properties and its Role in Formulation Development and Processing', in *Dosage Form Design Parameters*. Elsevier, pp. 221–256. Available at: https://doi.org/10.1016/B978-0-12-814421-3.00006-3.

Moyer, T.C. and Swanson, D.A. (1987) *SECONDARY HYDROERUPTIONS IN PYROCLASTIC-FLOW DEPOSITS: EXAMPLES FROM MOUNT ST. HELENS*, *Journal of Volcanology and Geothermal Research*, pp. 299–319.

Pacheco-Hoyos, J.G., Aguirre-Díaz, G.J. and Dávila-Harris, P. (2020) 'Elutriation pipes in ignimbrites: An analysis of concepts based on the Huichapan Ignimbrite, Mexico', *Journal of Volcanology and Geothermal Research*, 403. Available at : https://doi.org/10.1016/j.jvolgeores.2020.107026.

Pepin, N.C. *et al.* (2017) 'A comparison of simultaneous temperature and humidity observations from the SW and NE slopes of Kilimanjaro: The role of slope aspect and differential land-cover in controlling mountain climate', *Global and Planetary Change*, 157, pp. 244–258. Available at: https://doi.org/10.1016/j.gloplacha.2017.08.006.

Pierrat, P. and Caram, H.S. (1997) 'Tensile strength of wet granular materials.

Riehle, J.R., Miller, T.F. and Bailey, R.A. (1995) 'Cooling, degassing and compaction of rhyolitic ash flow tufts: a computational model'.

Rios, Maribel. (2006) 'Developments in powder flow testing', Pharmaceutical Technology, 30 (2), pp. 38-49.

Roche, O., Druitt, T.H. and Cas, R.A.F. (2001) 'Experimental aqueous Fluidization of ignimbrite', *Journal of Volcanology and Geothermal Research*, p. 14.

Rogers, R. (2015) 'Hydrate-associated seafloor instabilities', *Offshore Gas Hydrates*, pp. 189–219. doi:10.1016/b978-0-12-802319-8.00006-1.

Sahoo, S. *et al.* (2022) 'Eruption cycles of Mount Etna triggered by seasonal climatic rainfall', *Journal of Geodynamics*, 149. Available at: https://doi.org/10.1016/j.jog.2021.101896.

Schneider, C.A., Rasband, W.S. and Eliceiri, K.W. (2012) 'NIH Image to ImageJ: 25 years of image analysis', *Nature Methods*, 9, pp. 671–675.

Self, S. and Sparks, R.S.J. (1978) 'Characteristics of Widespread Formed by the Interaction of Silicic Magma and Water Pyroclastic Deposits', *Bulletin of Volcanology*, 41, pp. 196–212.

Smith, G. M. (2020). Propagation of aerated pyroclastic density current analogues: flow behaviour and the formation of bedforms and deposits. (Thesis). University of Hull.

SPARKS, R.S.J. (1976) 'Grain size variations in ignimbrites and implications for the transport of pyroclastic flows', *Sedimentology*, 23(2), pp. 147–188. Available at: https://doi.org/10.1111/j.1365-3091.1976.tb00045.x.

Sparks, R.S.J. (1978) 'Gas release rates from pyroclastic flows: a assessment of the role of fluidisation in their emplacement', *Bulletin Volcanologique*, 41(1), pp. 1–9. Available at: https://doi.org/10.1007/BF02597679.

Telling, J., Dufek, J. and Shaikh, A. (2013) 'Ash aggregation in explosive volcanic eruptions', *Geophysical Research Letters*, 40(10), pp. 2355–2360. Available at: https://doi.org/10.1002/grl.50376.

Van Eaton, A.R. and Wilson, C.J.N. (2013) 'The nature, origins and distribution of ash aggregates in a large-scale wet eruption deposit: Oruanui, New Zealand', *Journal of Volcanology and Geothermal Research*, 250, pp. 129–154. Available at : https://doi.org/10.1016/j.jvolgeores.2012.10.016.

Vecino, M.C.D. *et al.* (2022) 'OPEN Aerodynamic characteristics and genesis of aggregates at Sakurajima Volcano, Japan', *Scientific Reports*, p. 14.

van Westen, C.J. and Daag, A.S. (2005) 'Analysing the relation between rainfall characteristics and lahar activity at Mount Pinatubo, Philippines', *Earth Surface Processes and Landforms*, 30(13), pp. 1663–1674. Available at: https://doi.org/10.1002/esp.1225.

Wilson, C.J.N. (1980) *THE ROLE OF FLUIDIZATION IN THE EMPLACEMENT OF PYRO-CLASTIC FLOWS: AN EXPERIMENTAL APPROACH*, *Journal of Volcanology and Geothermal Research*, pp. 231–249.

Wilson, C.J.N. (1984) 'The role of fluidization in the emplacement of pyroclastic flows, 2: Experimental results and their interpretation', *Journal of Volcanology and Geothermal Research*, 20(1–2), pp. 55–84. Available at: https://doi.org/10.1016/0377-0273(84)90066-0.

Wormsbecker, M. and Pugsley, T. (2008) 'The influence of moisture on the fluidization behaviour of porous pharmaceutical granule', *Chemical Engineering Science*, 63(16), pp. 4063–4069. Available at: https://doi.org/10.1016/j.ces.2008.05.023.

Yehuda, T., & Kalman, H. (2020). Geldart classification for wet particles. *Powder Technology*, *362*, 288–300. https://doi.org/10.1016/j.powtec.2019.11.073

Yu, A.B. and Hall, J.S., 1994 'Packing of fine powders subjected to tapping', p. 10.

Zeng, K. *et al.* (2017) 'Combined effects of initial water content and heating parameters on solar pyrolysis of beech wood', *Energy*, 125, pp. 552–561. Available at: https://doi.org/10.1016/j.energy.2017.02.173.